First-principles study of the optical properties of $Mg_xTi_{1-x}H_2$

Michiel J. van Setten
Electronic Structure of Materials, Institute for Molecules and Materials, Faculty of Science, Radboud University Nijmegen, Heyendaalseweg 135, 6525 AJ Nijmegen, The Netherlands and Institut für Nanotechnologie, Forschungszentrum Karlsruhe, P.O. Box 3640, D-76021 Karlsruhe, Germany

Süleyman Er and Geert Brocks
Computational Materials Science, Faculty of Science and Technology and MESA+ Institute for Nanotechnology, University of Twente, P.O. Box 217, 7500 AE Enschede, The Netherlands

Robert A. de Groot
Electronic Structure of Materials, Institute for Molecules and Materials, Faculty of Science, Radboud University Nijmegen, Heyendaalseweg 135, 6525 AJ Nijmegen, The Netherlands and Laboratory of Solid State Chemistry, Zernike Institute for Advanced Materials, Rijksuniversiteit Groningen, Nijenborgh 4, 9747 AG Groningen, The Netherlands

Gilles A. de Wijs*
Electronic Structure of Materials, Institute for Molecules and Materials, Faculty of Science, Radboud University Nijmegen, Heyendaalseweg 135, 6525 AJ Nijmegen, The Netherlands

(Received 19 December 2008; revised manuscript received 26 February 2009; published 27 March 2009)

Thin films of Mg_xTi_{1-x} show an optical black state upon hydrogenation. We calculate the dielectric function and the optical properties of $Mg_xTi_{1-x}H_2$, $x=0.5$, 0.75, and 0.875 using first-principles density-functional theory. We argue that the black state is an intrinsic property of these compounds, unlike similar optical phenomena observed in other metal hydride films. The structures of $Mg_xTi_{1-x}H_2$ are represented either by simple ordered or quasirandom structures. The density of states has a broad peak at the Fermi level, composed of Ti *d* states; hence, both interband and intraband transitions contribute to the optical response. Ordered structures have a plasma frequency of ~ 3 eV. The plasma frequency drops below 1 eV in disordered structures, which—as a result of interband transitions—then show a low reflection and considerable absorption in the energy range of 1–6 eV, i.e., a black state.

DOI: 10.1103/PhysRevB.79.125117 PACS number(s): 71.20.−b, 71.15.Nc, 61.72.Bb, 74.62.Dh

I. INTRODUCTION

Since the discovery of the switchable mirror YH_x by Huiberts *et al.*[1] in 1996, several other metal hydrides that act as switchable mirror materials have been discovered.[1–6] The metals are reflective, but after hydrogenation become insulators, and hence in most cases transparent.[7–10] Especially if an alloy with high hydrogen mobility is used and applied in thin films, the optical switching can be fast, reversible, and robust.[11]

Recently, metastable thin films composed of various composition ratios of magnesium and titanium have been shown to exhibit remarkable optical properties which could be especially useful for smart solar cell coatings and hydrogen sensor applications.[6,12–14] In the dehydrogenated state the films are highly reflective. Upon hydrogenation they become black, i.e., they have a low reflection and high absorption in the energy range of the solar spectrum. The structure of these Mg-Ti compounds and the origin of the black state are a topic of intensive research.[15–17]

Obtaining structural data for these systems is difficult. Single crystals cannot be grown under standard conditions, as bulk Mg-Ti alloys, as well as their hydrides, are thermodynamically unstable. Kyoi and co-workers managed to synthesize a crystalline bulk compound Mg_7TiH_y $(y=13-16)$ under high pressure,[18] with a structure similar to that of the fluorite TiH_2 structure.[19] In contrast, thin films of Mg_xTi_{1-x} can be grown readily for any composition x. These can be hydrogenated reversibly without loosing their structure. The equality of the molar volumes of TiH_2 and Mg has been used to explain the structural stability of these metastable thin film alloys.[15,16] Notten and co-workers[20–22] and Borsa *et al.*[6,15] showed that for a high titanium content, $x \lesssim 0.8$, the structure of the hydrides is fluoritelike. Hydrides with a lower titanium content adopt a rutilelike structure, similar to that of α-MgH_2. Density-functional theory (DFT) calculations confirm the dependence of the relative stability of the rutile and fluorite structures on the Mg-Ti composition.[17,23,24] Interestingly, the kinetics of the hydrogen ab/desorption reactions are much faster in the alloys with a high Ti content.[25]

The origin of the optical black state in hydrogenated Mg-Ti thin films is not understood. Other magnesium–transition-metal hydrides also show an optical black state,[3,5] but its origin is quite different. Transition-metal atoms such as Fe, Co, and Ni form closed-shell complexes upon full hydrogenation, and the hydrides are semiconductors.[10] The black state that occurs during hydrogenation of Mg_2Ni thin films is explained in terms of a double layer of semiconducting Mg_2NiH_4 and metallic $Mg_2NiH_{0.3}$.[5]

The situation is different for Mg-Ti hydrides. In experiments, usually somewhat less than two hydrogen atoms per metal atom are absorbed.[15] Electrochemically 1.7 hydrogen

atoms per metal atom can be absorbed and desorbed reversibly.[25] The high-pressure crystalline phase Mg_7TiH_{16} contains two hydrogen atoms per metal atom.[19] This means that maximally two electrons per metal atom can be transferred to hydrogen.[15] Since Ti atoms have four valence electrons ($3d^24s^2$) this suggests that they remain in an open-shell configuration.

The open-shell character is confirmed by DFT calculations on $Mg_xTi_{1-x}H_2$. The calculated densities of states show a predominant hydrogen-*s* character below the Fermi level, which is typical for metal hydrides, where electrons are transferred to the hydrogen atoms.[9,10,26] However, unlike the closed-shell hydrides, in $Mg_xTi_{1-x}H_2$ a considerable density of states (DOS) is found at the Fermi level, which is mainly composed of titanium-*d* states. This suggests a metallic response and one might naively expect $Mg_xTi_{1-x}H_2$ to be reflective instead of black. One should, however, not "jump to conclusions," but build on an quantitative analysis of the optical response that includes all potentially relevant physics. Here we calculate the macroscopic dielectric functions, taking into account the effects of inter- and intraband contributions and how these are affected by structural disorder. We propose that the optical black state is an intrinsic property of the (homogeneous) bulk material $Mg_xTi_{1-x}H_2$, i.e., unlike the black state occurring in the hydrogenation of Mg_2Ni. The latter is a property of an inhomogeneous thin film, which results from phase separation into Mg_2NiH_4 and $Mg_2NiH_{0.3}$ grains.[5]

The electronic structure and the optical properties of $Mg_xTi_{1-x}H_2$ are calculated from first-principles for $x=0.5$, 0.75, and 0.875, employing two different types of structures. The first type consists of highly ordered Mg-Ti structures that are similar to the high-pressure bulk phase. In the second type we build in disorder. These are model random alloys where the Mg and Ti are distributed over the fcc lattice sites of a TiH_2-like structure. To model the optical response of $Mg_xTi_{1-x}H_2$, we calculate the dielectric function, consisting of interband and intraband contributions,

$$\varepsilon(\omega) = \varepsilon_{\text{inter}}(\omega) + \varepsilon_{\text{intra}}(\omega), \tag{1}$$

which are obtained separately. For the interband contribution $\varepsilon_{\text{inter}}$ we use first-principles DFT in the independent particle approximation. The intraband contribution $\varepsilon_{\text{intra}}$ is modeled by a free-electron model, which contains the plasma frequency ω_p calculated from first principles. From the dielectric function we obtain the absorption and reflection of $Mg_xTi_{1-x}H_2$.

In Sec. II the technical details of the calculations are summarized. Section III contains a short description of the structural models used. Details of these models are presented in Ref. 17. Results on the dielectric functions are presented in Sec. IV. Finally, in Sec. V we discuss the intrinsic optical properties of $Mg_xTi_{1-x}H_2$ and compare our results to experiment.

II. COMPUTATIONAL DETAILS

First-principles DFT calculations are carried out with the Vienna *Ab initio* Simulation Package (VASP),[27–29] using the projector augmented wave (PAW) method.[30,31] A plane-wave basis set is used and periodic boundary conditions are applied. The plane-wave kinetic-energy cutoff on the wave functions is 310 eV. For the exchange-correlation functional we use the PW91 generalized gradient approximation (GGA).[32] Nonlinear core corrections are applied.[33]

The Brillouin-zone integrations are performed using a Gaussian smearing method with a width of 0.1 eV.[34] We use **k**-point grids containing Γ and other high-symmetry points so that the band extrema are typically included in the calculation of the dielectric functions. The convergence of the dielectric functions and intraband plasma frequencies with respect to the **k**-point meshes is tested by increasing the number of **k** points for each system separately. A typical mesh spacing of about 0.01 Å^{-1} is needed to obtain converged results.

The calculations of the complex interband dielectric functions, $\varepsilon_{\text{inter}}(\omega)=\varepsilon^{(1)}_{\text{inter}}(\omega)+i\varepsilon^{(2)}_{\text{inter}}(\omega)$, are performed in the independent particle picture, taking into account only direct transitions from occupied to unoccupied Kohn-Sham orbitals. Local-field effects are neglected. The imaginary part of the macroscopic dielectric function $\varepsilon^{(2)}_{\text{intra}}(\omega)$ is, according to the standard longitudinal expression,[35]

$$\varepsilon^{(2)}_{\text{inter}}(\hat{\mathbf{q}},\omega) = \frac{8\pi^2e^2}{V}\lim_{|\mathbf{q}|\to 0}\frac{1}{|\mathbf{q}|^2}\sum_{\mathbf{k},v,c}|\langle u_{c,\mathbf{k}+\mathbf{q}}|u_{v,\mathbf{k}}\rangle|^2 \times \delta(\epsilon_{c,\mathbf{k}+\mathbf{q}}-\epsilon_{v,\mathbf{k}}-\hbar\omega), \tag{2}$$

where $\hat{\mathbf{q}}$ denotes the direction of $\mathbf{q}$ and $(v,\mathbf{k}+\mathbf{q})$ and $(c,\mathbf{k})$ label single-particle states that are occupied and unoccupied in the ground state, respectively, ϵ are the single-particle energies, u are the translationally invariant parts of the wave functions, and V is the volume of the unit cell. The real part of the dielectric function, $\varepsilon^{(1)}_{\text{inter}}(\omega)$, is obtained via a Kramers-Kronig transform of the imaginary part. Details can be found in the paper by Gajdoš *et al.*[35] Most optical data on hydrides are obtained from micro- and nanocrystalline samples whose crystallites have a significant spread in orientation. Therefore the most relevant quantity is the directionally averaged dielectric function, i.e., $\varepsilon^{(2)}_{\text{inter}}(\omega)$ averaged over $\hat{\mathbf{q}}$.

The intraband dielectric function, $\varepsilon_{\text{intra}}(\omega)=\varepsilon^{(1)}_{\text{intra}}(\omega)+i\varepsilon^{(2)}_{\text{intra}}(\omega)$, is calculated from a standard free-electron plasma model

$$\varepsilon^{(1)}_{\text{intra}}(\omega) = 1-\frac{\omega_p^2}{\omega^2+\gamma^2}, \tag{3}$$

$$\varepsilon^{(2)}_{\text{intra}}(\omega) = \frac{\gamma\omega_p^2}{\omega^3+\omega\gamma^2}. \tag{4}$$

The plasma frequency ω_p is obtained from first principles (see below). Calculating the inverse lifetime γ goes beyond an independent particle approximation, so we treat γ as a parameter. For $\gamma=0$ the reflection as a function of the frequency would be perfect up to the plasma frequency and zero beyond. A finite value of γ decreases the reflection below ω_p and smoothens the reflection edge at ω_p. To illustrate the effect of varying γ the free electron $\varepsilon_{\text{intra}}$ is plotted in Fig. 1

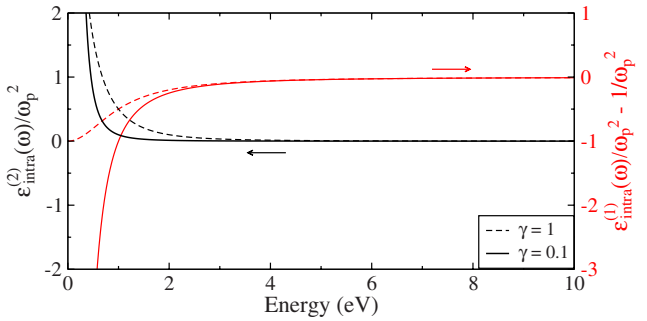

FIG. 1. (Color online) Scaled dielectric functions of a free-electron gas for $\hbar\gamma=0.1$ eV and $\hbar\gamma=1$ eV, as function of the energy $\hbar\omega$. The right (left) axis refers to the real, in red (imaginary, in black), part of the dielectric functions.

for different values of γ. For metals typical experimental values are $\hbar\gamma\sim 0.1$ eV. In the results presented here we use a small value, $\hbar\gamma=0.01$ eV, which does not blur the structure of the optical response function.

The plasma frequency tensor can be calculated from first principles as an integral over the Fermi surface according to

$$\omega^2_{p(\alpha\beta)} = -\frac{4\pi e^2}{V\hbar^2}\sum_{n,\mathbf{k}} 2g_{\mathbf{k}}\frac{\partial f(\epsilon_{n\mathbf{k}})}{\partial\epsilon}\left(\mathbf{e}_\alpha\frac{\partial\epsilon_{n\mathbf{k}}}{\partial\mathbf{k}}\right)\left(\mathbf{e}_\beta\frac{\partial\epsilon_{n\mathbf{k}}}{\partial\mathbf{k}}\right) \quad (5)$$

where $g_{\mathbf{k}}$ are the weight factors of the $\mathbf{k}$ points, $f(\epsilon_{n\mathbf{k}})$ is the Fermi-Dirac occupation function, and $\mathbf{e}_\alpha$ and $\mathbf{e}_\beta$ are unit vectors in the α and β directions.[36,37] For details we refer to the paper by Harl *et al.*[36] Again directionally averaged quantities are used.

The optical functions of a bulk material, i.e., the refractive index n and the extinction coefficient κ, are obtained from the dielectric function via the usual relation $\varepsilon^{(1)}+i\varepsilon^{(2)}=(n+i\kappa)^2$ and the optical coefficients (absorption, reflection, and transmission) are calculated from n,κ using the standard expressions.

III. STRUCTURES

To model the effect of the structure of $Mg_xTi_{1-x}H_2$ on the optical properties we use two different approaches. The first one is based on simple ordered structures similar to the structure of Mg_7TiH_{16} found in Refs. 18 and 19. This is a Ca_7Ge-type structure with the metal atoms in fcc positions. The H atoms are in tetrahedral interstitial sites, but displaced from their ideal positions. We use this structure to model the composition $x=0.875$. It can be used as a starting point to construct similar structures for other compositions. For $x=0.75$ we start from the Cu_3Au ($L1_2$) structure, and for $x=0.5$ from the CuAu ($L1_0$) structure with the H atoms at tetrahedral interstitial positions. For each of the compositions the cell parameters are optimized, as well as the positions of all atoms within the cell. Care is taken to allow for breaking the symmetry in the atomic positions. In particular the hydrogen atoms are often displaced from their ideal tetrahedral positions. Some of the structural parameters are given in Table I; further details can be found in Ref. 17. We call these the "ordered structures" in the following.

The crystal structure of $Mg_xTi_{1-x}H_y$ as deposited in thin films is cubic with Mg and Ti atoms at fcc positions, but without a regular ordering of Mg and Ti atoms at these positions.[15] To model the effect of disorder on the optical properties, our second approach is based on special quasirandom structures, which enable to model random alloys in a finite supercell.[38,39] At each composition a supercell is chosen and the Mg and Ti are placed at fcc positions in such a way that the lower-order correlation functions of their distributions are equal to those of a random alloy. For the compositions $x=0.5$ and 0.75 modeled in a 32-atom supercell, all pair correlation functions are exact up to third nearest-neighbor atoms.[40] The composition $x=0.875$ can be modeled in a 64-atom supercell to obtain correct pair correlation functions up to seventh nearest neighbors. We insert hydrogen atoms in tetrahedral interstitial positions to generate $Mg_xTi_{1-x}H_2$, which leads to supercells with a total number of atoms of 96 and 192, respectively. Again all cell parameters are optimized, as well as the positions of all atoms within the cell.[17] The cells remain close to cubic (see Table I). We call these the "disordered structures" in the following.

The shortest Ti-Ti distance in the quasirandom structures corresponds to that of next-nearest neighbors in the fcc lattice. In the ordered structures the Ti-Ti distance increases as the Ti content decreases.

IV. DIELECTRIC FUNCTIONS

A. Interband dielectric functions

Figures 2 and 3 show the calculated imaginary parts of the *interband* contribution to the dielectric functions of the or-

TABLE I. Number of formula units (Z), lattice parameters (Å), and shortest Ti-Ti interatomic distances (Å). For each composition x the first row refers to the unit cell of the ordered structure and the second line refers to the cell representing the quasirandom structure.

x	Z	a	b	c	Ti-Ti
0.5	4	4.72	4.72	4.65	3.16
	32	9.08	9.03	9.09	3.15
0.75	4	4.62	4.62	4.62	4.62
	32	9.29	9.30	9.27	3.13
0.875	32	9.36	9.36	9.36	6.62
	64	18.75	9.42	9.73	3.08

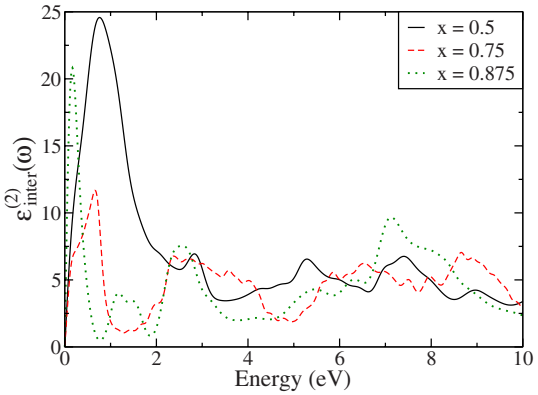

FIG. 2. (Color online) Imaginary parts of the interband dielectric functions of $Mg_xTi_{1-x}H_2$ in the ordered structures.

dered and the disordered structures of $Mg_xTi_{1-x}H_2$, respectively. Most dielectric functions exhibit a peak at low energy, i.e., $\hbar\omega \lesssim 1$ eV, followed by a relatively flat tail in the range of 2–10 eV. In general, the strength of the peak decreases with increasing magnesium content x. In particular for the disordered structure the peak vanishes for $x=0.875$. The dielectric functions of the disordered structures are much smoother, as compared to those of the ordered structures.

To understand the main features of the dielectric functions we start from the DOSs as shown in Fig. 4. Below the Fermi level the DOSs are dominated by a broad peak starting at ~ -10 eV, which has a predominant hydrogen-s character. The structure around the Fermi level mainly results from titanium-d states. The unoccupied states have a mixed character of hydrogen s and p, magnesium s and p, and titanium d. To illustrate the character of the DOSs, the atomic angular-momentum-projected DOS of $Mg_{0.75}Ti_{0.25}H_2$ in the simple ordered structure is shown in Fig. 5 as an example.

From the analysis of the DOSs one expects that low-energy optical excitations have a contribution of transitions between titanium-d states,[41] whereas for excitations at higher-energy transitions from hydrogen-s to hydrogen-p states contribute.

If one neglects variations in oscillator strength, the imaginary part of the dielectric function of Eq. (2) can be rewritten

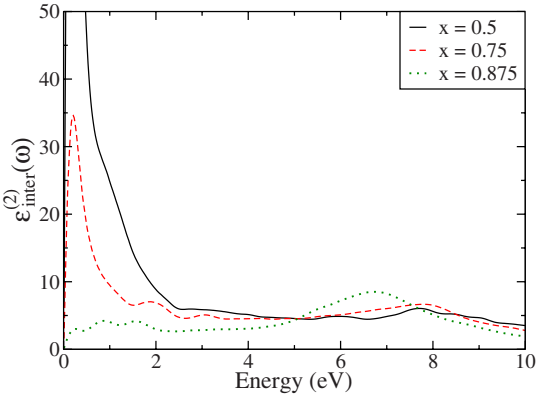

FIG. 3. (Color online) Imaginary parts of the interband dielectric functions of $Mg_xTi_{1-x}H_2$ in the disordered structures. For $x=0.5$ the dielectric function peaks to a value of 130.

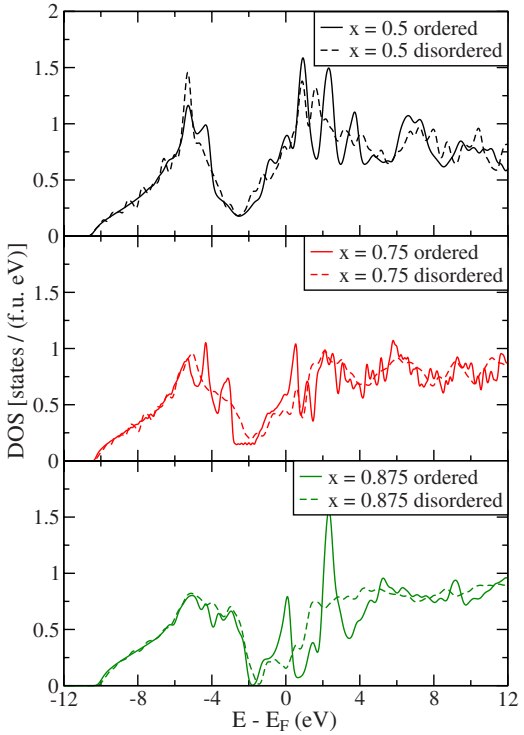

FIG. 4. (Color online) Electronic densities of state of the ordered and disordered structures for the three compositions of $Mg_xTi_{1-x}H_2$. The zero of energy is at the Fermi level.

in transversal form as the joint density of states (JDOS) divided by ω^2.[35] Assuming that Ti d-d transitions are very weak, we subtract the Ti d peak from the DOS. The resulting DOS then has a dip near the Fermi energy. It increases going both to lower and to higher energies. The JDOS then increases more than linearly in the region from 0 to 10 eV. If we divide the JDOS by ω^2 this increase is rather effectively canceled out. Hence the imaginary part of the dielectric function does not vary much in the interval from 2 to 8 eV. This reasoning is independent of the Ti concentration, which explains why the dielectric function in this interval does not strongly depend upon it. As the DOSs of the disordered structures are much smoother than those of the ordered structures (see Fig. 4), the corresponding dielectric functions are also much smoother.

The peaks in the dielectric function at low energy ($\hbar\omega \lesssim 1$ eV) arise from Ti d-d transitions.[41] Although the oscillator strengths of these transitions are much smaller than those of hydrogen s-p transitions, the division by ω^2 nevertheless results in a blowup in the low-energy part of the spectrum. With increasing x in $Mg_xTi_{1-x}H_2$ the amount of Ti decreases, with a concomitant decrease in low-energy peaks, as is clearly observed in Figs. 2 and 3. The low-energy peaks in the disordered structures are generally more pronounced than in the ordered structures. Disorder results in a spectrum of much flatter closely spaced bands (see Sec. IV B). Some of these bands are very close to the Fermi energy and transitions between such bands are boosted, both by the flatness of the bands and the small ω.

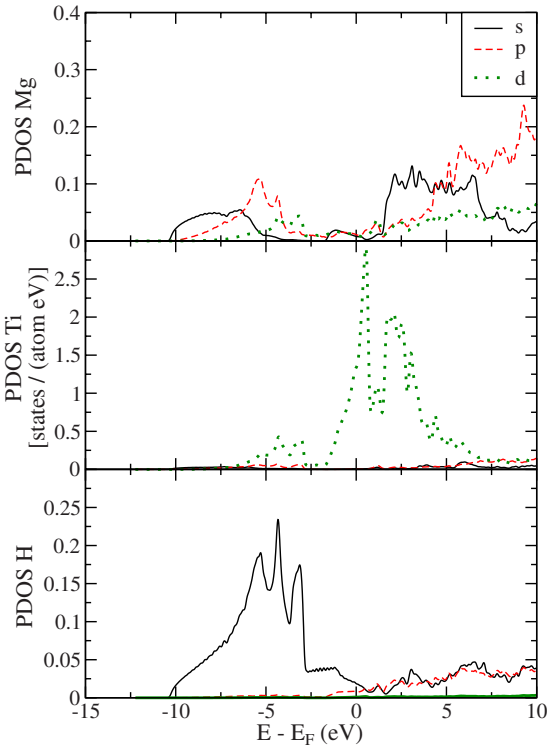

FIG. 5. (Color online) Angular-momentum-projected partial densities of states (PDOSs) [states/(atom eV)] of $Mg_{0.75}Ti_{0.25}H_2$ in the ordered structure. The zero of energy is at the Fermi level. The PDOS is calculated using spheres with radii of 1.3, 1.3, and 0.8 Å for Mg, Ti, and H, respectively.

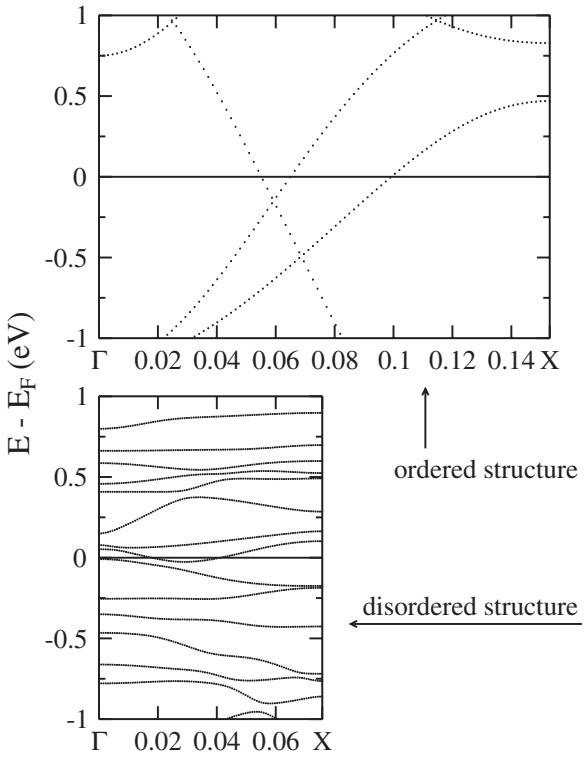

FIG. 6. Band structure of $Mg_{0.75}Ti_{0.25}H_2$ along the Γ-X direction in the unit cells used for the ordered (top) and the disordered (bottom) structures. The scales on the abscissa are identical.

B. Intraband plasma frequencies

The intraband dielectric response function given by Eq. (3) critically depends on the plasma frequency [cf. Eq. (5)]. Table II lists the plasma frequencies calculated for the ordered and disordered structures of $Mg_xTi_{1-x}H_2$ for different compositions x. The plasma frequencies of the ordered structures are relatively high, $\hbar\omega_p \sim 3$ eV; hence, one expects that these systems should be highly reflective for $\hbar\omega \lesssim 3$ eV, i.e., for light in the visible range. In contrast, the plasma frequencies of the disordered structures are much lower, i.e., $\hbar\omega_p \lesssim 1$ eV. Disorder on the atomic scale could therefore dramatically alter the reflective properties of $Mg_xTi_{1-x}H_2$ for light in the visible range. To obtain the complete picture, the intraband and interband effects should be combined. This is done in Sec. V. In the remainder of this section we discuss the trends observed in Table II.

From Eq. (5) it is observed that the plasma frequency (squared) is proportional to the slope of the energy bands (squared) and the electron density, both at the Fermi level. As the electrons at the Fermi level are titanium-d electrons, the corresponding electron density in $Mg_xTi_{1-x}H_2$ decreases with increasing x. Therefore, the plasma frequency generally decreases with increasing x. For the disordered structures this trend is obvious, but for the ordered structures it is less clear. Subtle changes in the shape of the DOS, i.e., band-structure effects caused by a particular ordering of the titanium atoms, obstruct the general trend.

TABLE II. Plasma frequencies $\hbar\omega_p$ (eV) from intraband transitions.

	Ordered	Disordered
x=0.5	3.3	1.1
x=0.75	3.6	0.6
x=0.875	2.9	0.3

The difference in plasma frequency between the ordered and the disordered structures of the same composition stems from a marked difference in the slope of the energy bands. As an example the band structures of $Mg_{0.75}Ti_{0.25}H_2$, for both the "ordered" and "disordered" structures, are plotted in Fig. 6 using the unit cells described in Sec. III. The cell parameter of the cell used to model the disordered structure is twice that of the cell describing the ordered structure. The band structure of the disordered structure, however, cannot be interpreted as a simple backfolding of the bands of the ordered structure. The positional disorder of the titanium atoms in the structure has introduced interactions between the d bands, leading to a dramatic reduction in their slopes and hence of the plasma frequency. The finite unit cell used to represent a disordered structure, of course, cannot model a truly random structure exactly, which means that for the latter the reduction may even be stronger.

The flatness of the bands introduced by the positional disorder of the titanium atomic positions in $Mg_xTi_{1-x}H_2$ can also be interpreted in terms of a high effective mass of the titanium-d electron, or a possible localization of those elec-

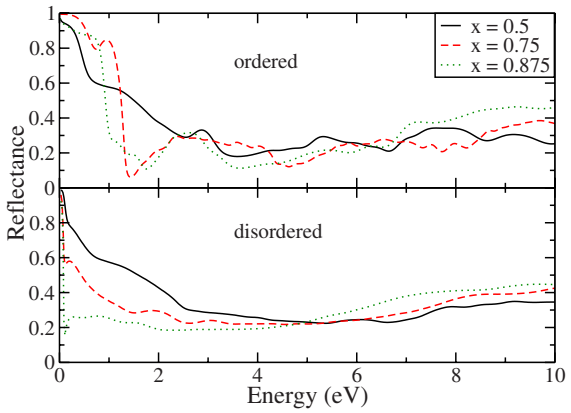

FIG. 7. (Color online) Reflectance spectra of $Mg_xTi_{1-x}H_2$ at normal incidence in the ordered structures and disordered structures. The bulk dielectric function is used to calculate these spectra.

trons. Such an interpretation is consistent with the decrease in the plasma frequency of the disordered structures as compared to the ordered structures.

V. DISCUSSION

To obtain the complete dielectric functions of $Mg_xTi_{1-x}H_2$ we add the interband part (cf. Fig. 2 or Fig. 3), and the intraband part with ω_p from Table II according to Eq. (1). We analyze the results with the help of the calculated reflection spectra (Fig. 7) and absorption coefficients (Fig. 8). Next we make contact with a specific experimental setup and discuss also the transmission.

Figure 7 shows the reflectance spectra of (semi-infinite) $Mg_xTi_{1-x}H_2$ at normal incidence. The upper part pertains to the ordered structures. For a plasma the reflection below ω_p ($\hbar\omega_p \sim 3$ eV) would be perfect. We see that the reflection is already considerably suppressed at much lower energy, with a clear reflection edge occurring near 1 eV for $x=0.5$ and $x=0.75$, showing the importance of the interband transitions in these materials. The reflection of the disordered structures reveals two effects: (i) as the interband dielectric function becomes smooth, the reflectance exhibits little structure and becomes rather smooth and (ii) in the disordered structures

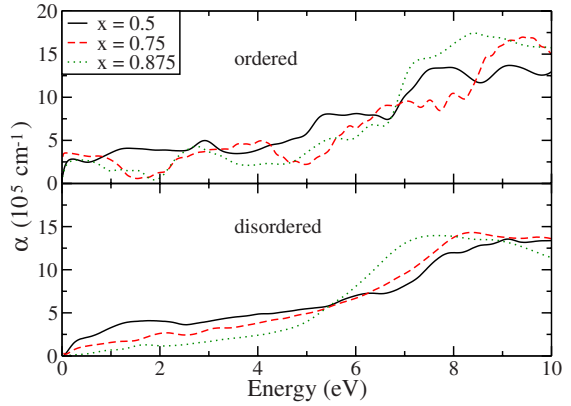

FIG. 8. (Color online) Absorption coefficients $\alpha(\omega) = 2\kappa(\omega)\omega/c$ of $Mg_xTi_{1-x}H_2$ in the ordered and disordered structures.

the clear reflection edge near 1 eV disappears. Instead one observes a gradual decrease in the reflection as a function of energy to reach a low value that only weakly depends upon the composition. With increasing x (decreasing Ti content) there is a strong suppression of the energy dependence of the reflection. For $x=0.875$ the reflection remains small and structureless to energies as low as 0.2 eV. The reflection spectrum of the disordered structures is dominated by the intraband dielectric function. If we remove the plasma contribution from the dielectric function, the reflectance spectra are practically unaffected for energies above 0.2 eV. In fact, the plasma frequencies for the disordered structures are so low that their effect is only apparent in the steep increase toward 1 when the $\hbar\omega$ drops below 0.2 eV.

Figure 8 depicts the absorption coefficients $\alpha = 2\kappa\omega/c$ of $Mg_xTi_{1-x}H_2$. Again, the curves pertaining to the disordered structures are much smoother. We limit the discussion to those in the following. The absorption increases with decreasing x, i.e., with increasing Ti content for energies up to 5.5 eV. The parent compound α-MgH_2 is an insulator with a band gap close to 6 eV.[9,42] The band gap of the cubic phase β-MgH_2 is smaller by ~ 1 eV,[17] which means that it is still a large band-gap material without absorption in the visible range. As discussed in Sec. IV A, upon introduction of Ti atoms in the lattice, the gap in the DOS is filled, not only by Ti states, but also by H states. The hydrogen atoms in $Mg_xTi_{1-x}H_2$ have different local environments, which produce a broadening and smoothening of the DOS. As a result, the $Mg_xTi_{1-x}H_2$ compounds have a significant absorption over the whole visible range and a "black" appearance.

Absorption coefficients have been extracted from experiments on thin films of $Mg_xTi_{1-x}H_2$ deposited on a quartz substrate and covered by a thin layer of Pd [see Fig. 2(c) in Ref. 15]. A comparison to our calculations can only be made indirectly since the experiments have been performed on compositions $x=0.7$, 0.8, and 0.9, which are different from ours. Modeling quasirandom structures with such compositions would require prohibitively large supercells. We can average the experimental absorption coefficients for $x=0.7$ and 0.8 and compare the results to the calculated $x=0.75$ curve in Fig. 8. The experimental values are then $\sim 30\%$ lower over the whole frequency range. This difference reflects both the approximations made in the calculations and in the extraction of the experimental values. However, the frequency dependence and the composition dependence of the calculated and experimental absorption coefficients are very similar.

We have also calculated the normal incidence transmittance and reflection spectra of thin films as used in the experiments of Refs. 6 and 15, i.e., 10 nm palladium/200 nm $Mg_xTi_{1-x}H_2$/quartz substrate, taking all internal reflections and absorptions of the layers into account (Fig. 9). The shape of the calculated reflectance curves (not shown) as function of frequency is very similar to those in Fig. 7. The reflectance curves of the disordered structures and their compositional dependence are very similar to those given in Ref. 15. Overall, the reflection of these thin films is somewhat lower than that of bare thick films. For instance, the plateau in the reflectance for $\hbar\omega > 3$ eV in the disordered $x=0.75$ structure drops to 14%. This is $\sim 5\%$ higher than the experimental

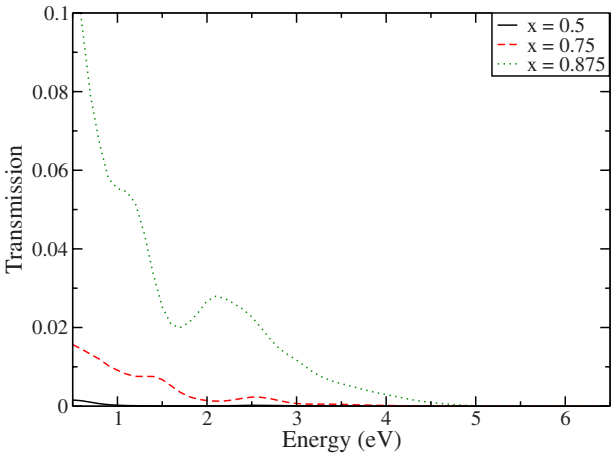

FIG. 9. (Color online) Transmission at normal incidence of a 10 nm palladium/200 nm $Mg_xTi_{1-x}H_2$ film on a quartz substrate. The calculations are based on the disordered structures.

value, which is partly due to the higher value for the calculated absorption coefficient (see above). The experimental transmission drops from 6.5% to 0% in the range of 0.5–3 eV. Hence it is about a factor of 3 higher than calculated (Fig. 7), which again can be traced back to the difference in absorption coefficient. The shapes of the calculated transmission curves, however, show good agreement with experiment.

In conclusion, we have calculated the optical properties of $Mg_xTi_{1-x}H_2$ (x=0.5,0.75,0.875) from first principles. We argue that the "black state" observed experimentally is an intrinsic property of the homogeneous compounds. This is in contrast to similar black states observed during hydrogenation of intermetallic compounds such as Mg_2Ni, which stem from macroscopic inhomogeneities caused by phase separation into Mg_2NiH_4 and $Mg_2NiH_{0.3}$ grains.

Disordered structures of $Mg_xTi_{1-x}H_2$ are represented by quasirandom structures in supercells, which model the positional disorder of Mg and Ti atoms. The hydrogen atoms have different local environments, and the corresponding DOS is relatively smooth and spread out over a large energy range. A broad peak around the Fermi level, mainly comprised of Ti d states, is present in the DOS, demonstrating the open-shell character of these atoms. The optical plasma edge resulting from free-electronlike transitions between such states lies significantly below the visible region, however, in particular for disordered structures. As an overall result, the $Mg_xTi_{1-x}H_2$ compounds have a significant absorption over the whole visible range and appear black. This is confirmed by simulations of the optical properties of thin films using the calculated dielectric functions, which show both a low reflection and a low transmission.

Recently it has been suggested that the structure of $Mg_xTi_{1-x}H_2$ involves a randomization of Mg and Ti positions on a somewhat larger length scale, with some concomitant increase in short-range order.[15,16] A first-principles study of such structures would involve very large unit cells beyond present computational capabilities. Comparing our calculations on simple ordered and on randomized structures we conclude, however, that the most important qualitative changes upon breaking perfect order are a lowering of the reflection edge and a smoothing of the spectrum, which we suggest also hold for the structures with some amount of short-range order.

ACKNOWLEDGMENTS

The authors thank G. Kresse and J. Harl (Universität Wien) for the use of the optical packages, A. V. Ruban (Technical University of Denmark, Lyngby) for his help and for making available his program to generate quasirandom structures, R. Gremaud (Vrije Universiteit Amsterdam) for simulations of the thin-film reflection and transmission, and A. Baldi (Vrije Universiteit Amsterdam) for making available Ref. 14 prior to publication. This work is part of the Sustainable Hydrogen Programme of the Advanced Catalytic Technologies for Sustainability (ACTS) and the Stichting voor Fundamenteel Onderzoek der Materie (FOM), both financially supported by the Nederlandse Organisatie voor Wetenschappelijk Onderzoek (NWO). The use of supercomputer facilities is sponsored by the Stichting Nationale Computerfaciliteiten (NCF).

*Corresponding author. g.dewijs@science.ru.nl

[1] J. N. Huiberts, R. Griessen, J. H. Rector, R. J. Wijnaarden, J. P. Dekker, D. G. de Groot, and N. J. Koeman, Nature (London) **380**, 231 (1996).

[2] P. van der Sluis, M. Ouwerkerk, and P. A. Duine, Appl. Phys. Lett. **70**, 3356 (1997).

[3] T. J. Richardson, J. L. Slack, R. D. Armitage, R. Kostecki, B. Farangis, and M. D. Rubin, Appl. Phys. Lett. **78**, 3047 (2001).

[4] J. Isidorsson, I. A. M. E. Giebels, R. Griessen, and M. Di Vece, Appl. Phys. Lett. **80**, 2305 (2002).

[5] W. Lohstroh, R. J. Westerwaal, B. Noheda, S. Enache, I. A. M. E. Giebels, B. Dam, and R. Griessen, Phys. Rev. Lett. **93**, 197404 (2004).

[6] D. M. Borsa, A. Baldi, M. Pasturel, H. Schreuders, B. Dam, R. Griessen, P. Vermeulen, and P. H. L. Notten, Appl. Phys. Lett. **88**, 241910 (2006).

[7] P. van Gelderen, P. A. Bobbert, P. J. Kelly, and G. Brocks, Phys. Rev. Lett. **85**, 2989 (2000).

[8] P. van Gelderen, P. A. Bobbert, P. J. Kelly, G. Brocks, and R. Tolboom, Phys. Rev. B **66**, 075104 (2002).

[9] M. J. van Setten, V. A. Popa, G. A. de Wijs, and G. Brocks, Phys. Rev. B **75**, 035204 (2007).

[10] M. J. van Setten, G. A. de Wijs, and G. Brocks, Phys. Rev. B **76**, 075125 (2007).

[11] W. Lohstroh, R. J. Westerwaal, J. L. M. van Mechelen, H. Schreuders, B. Dam, and R. Griessen, J. Alloys Compd. **430**, 13 (2007).

[12] M. Slaman, B. Dam, M. Pasturel, D. M. Borsa, H. Schreuders, J.

H. Rector, and R. Griessen, Sens. Actuators B **123**, 538 (2007).
[13] A. Baldi, D. M. Borsa, H. Schreuders, J. H. Rector, T. Atmakidis, M. Bakker, H. A. Zondag, W. G. J. van Helden, B. Dam, and R. Griessen, Int. J. Hydrogen Energy **33**, 3188 (2008).
[14] A. Baldi, R. Gremaud, D. M. Borsa, C. P. Baldé, A. M. J. van der Eerden, G. L. Kruijtzer, P. E. de Jongh, B. Dam, and R. Griessen, Int. J. Hydrogen Energy **34**, 1450 (2009).
[15] D. M. Borsa, R. Gremaud, A. Baldi, H. Schreuders, J. H. Rector, B. Kooi, P. Vermeulen, P. H. L. Notten, B. Dam, and R. Griessen, Phys. Rev. B **75**, 205408 (2007).
[16] R. Gremaud, A. Baldi, M. Gonzalez-Silveira, B. Dam, and R. Griessen, Phys. Rev. B **77**, 144204 (2008).
[17] S. Er, M. J. van Setten, G. A. de Wijs, and G. Brocks (unpublished).
[18] D. Kyoi, T. Sato, E. Ronnebro, N. Kitamura, A. Ueda, M. Ito, S. Katsuyama, S. Hara, D. Noreus, and T. Sakai, J. Alloys Compd. **372**, 213 (2004).
[19] E. Rönnebro, D. Kyoi, A. Kitano, Y. Kitano, and T. Sakai, J. Alloys Compd. **404-406**, 68 (2005).
[20] R. A. H. Niessen and P. H. L. Notten, Electrochem. Solid-State Lett. **8**, A534 (2005).
[21] P. Vermeulen, R. A. H. Niessen, D. M. Borsa, B. Dam, R. Griessen, and P. H. L. Notten, Electrochem. Solid-State Lett. **9**, A520 (2006).
[22] P. Vermeulen, H. J. Wondergem, P. C. J. Graat, D. M. Borsa, H. Schreuders, B. Dam, R. Griessen, and P. H. L. Notten, J. Mater. Chem. **18**, 3680 (2008).
[23] B. R. Pauw, W. P. Kalisvaart, S. X. Tao, M. T. M. Koper, A. P. J. Jansen, and P. H. L. Notten, Acta Mater. **56**, 2948 (2008).
[24] S. Er, D. Tiwari, G. A. de Wijs, and G. Brocks, Phys. Rev. B **79**, 024105 (2009).
[25] P. Vermeulen, R. A. H. Niessen, and P. H. L. Notten, Electrochem. Commun. **8**, 27 (2006).
[26] M. J. van Setten, G. A. de Wijs, V. A. Popa, and G. Brocks, Phys. Rev. B **72**, 073107 (2005).
[27] G. Kresse and J. Furthmüller, Phys. Rev. B **54**, 11169 (1996).
[28] G. Kresse and J. Furthmüller, Comput. Mater. Sci. **6**, 15 (1996).
[29] G. Kresse and J. Hafner, Phys. Rev. B **47**, 558 (1993).
[30] G. Kresse and D. Joubert, Phys. Rev. B **59**, 1758 (1999).
[31] P. E. Blöchl, Phys. Rev. B **50**, 17953 (1994).
[32] J. P. Perdew, J. A. Chevary, S. H. Vosko, K. A. Jackson, M. R. Pederson, D. J. Singh, and C. Fiolhais, Phys. Rev. B **46**, 6671 (1992).
[33] S. G. Louie, S. Froyen, and M. L. Cohen, Phys. Rev. B **26**, 1738 (1982).
[34] P. E. Blöchl, O. Jepsen, and O. K. Andersen, Phys. Rev. B **49**, 16223 (1994).
[35] M. Gajdoš, K. Hummer, G. Kresse, J. Furthmüller, and F. Bechstedt, Phys. Rev. B **73**, 045112 (2006).
[36] J. Harl, G. Kresse, L. D. Sun, M. Hohage, and P. Zeppenfeld, Phys. Rev. B **76**, 035436 (2007).
[37] K.-H. Lee and K. J. Chang, Phys. Rev. B **49**, 2362 (1994).
[38] A. Zunger, S.-H. Wei, L. G. Ferreira, and J. E. Bernard, Phys. Rev. Lett. **65**, 353 (1990).
[39] S.-H. Wei, L. G. Ferreira, J. E. Bernard, and A. Zunger, Phys. Rev. B **42**, 9622 (1990).
[40] A. V. Ruban, S. I. Simak, S. Shallcross, and H. L. Skriver, Phys. Rev. B **67**, 214302 (2003).
[41] These transitions have vanishing oscillator strength, in principle, as they are between states of the same ℓ. Because of hybridization with the surrounding atoms they nevertheless gain some strength.
[42] J. Isidorsson, I. A. M. E. Giebels, H. Arwin, and R. Griessen, Phys. Rev. B **68**, 115112 (2003).